Sea Ice–Albedo Climate Feedback Mechanism

JUDITH A. CURRY AND JULIE L. SCHRAMM

Program in Atmospheric Sciences, Department of Aerospace Engineering Sciences, University of Colorado, Boulder, Colorado

ELIZABETH E. EBERT

Bureau of Meteorology Research Center, Melbourne, Australia

(Manuscript received 16 June 1993, in final form 15 June 1994)

ABSTRACT

The sea ice–albedo feedback mechanism over the Arctic Ocean multiyear sea ice is investigated by conducting a series of experiments using several one-dimensional models of the coupled sea ice–atmosphere system. In its simplest form, ice–albedo feedback is thought to be associated with a decrease in the areal cover of snow and ice and a corresponding increase in the surface temperature, further decreasing the areal cover of snow and ice. It is shown that the sea ice–albedo feedback can operate even in multiyear pack ice, without the disappearance of this ice, associated with internal processes occurring within the multiyear ice pack (e.g., duration of the snow cover, ice thickness, ice distribution, lead fraction, and melt pond characteristics).

The strength of the ice–albedo feedback mechanism is compared for several different thermodynamic sea ice models: a new model that includes ice thickness distribution, the Ebert and Curry model, the Maykut and Untersteiner model, and the Semtner level-3 and level-0 models. The climate forcing is chosen to be a perturbation of the surface heat flux, and cloud and water vapor feedbacks are inoperative so that the effects of the sea ice–albedo feedback mechanism can be isolated. The inclusion of melt ponds significantly strengthens the ice–albedo feedback, while the ice thickness distribution decreases the strength of the modeled sea ice–albedo feedback. It is emphasized that accurately modeling present-day sea ice thickness is not adequate for a sea ice parameterization; the correct physical processes must be included so that the sea ice parameterization yields correct sensitivities to external forcing.

1. Introduction

It has been hypothesized that changes in surface albedo associated with changes in snow and ice cover as a result of temperature changes might provide a significant positive feedback on climate change (e.g., Kellog 1973). This climate feedback mechanism is generally referred to as the "snow/ice–albedo" feedback. As temperatures increase, the extent of snow and ice is reduced, decreasing the surface albedo and increasing the amount of sunlight that is absorbed by the earth–atmosphere system. Conversely, a temperature decrease will increase the surface albedo and thus reinforce the cooling. The ice–albedo feedback has been a particular subject of discussion in the context of greenhouse warming (e.g., Spelman and Manabe 1984; Dickinson et al. 1987; Washington and Meehl 1986; Ingram et al. 1989). Atmospheric models with doubled CO_2 concentrations have found that the warming is considerably amplified in the Arctic (e.g., Houghton et al. 1990). Most model projections of amplified polar warming are associated with a substantial retreat of sea ice, in some cases the summertime Arctic sea ice completely disappears. Chapman and Walsh (1993) have recently summarized 40 years of sea ice extent and surface temperatures in high latitudes and found that there are statistically significant indications in the Arctic that sea ice is becoming less extensive during the summer. The predicted and observed warming in the high latitudes have been at least partly attributed to the ice–albedo feedback mechanism.

Ingram et al. (1989) summarized different estimates of the strength of the snow/ice–albedo feedback mechanism as determined by different investigators using general circulation climate models. It was found that different estimates of the strength of the snow/ice–albedo feedback mechanism made by using different models and different experimental designs give substantially different results. It is difficult to compare simulations because some experiments exclude land effects and consider only sea ice, and some experiments include cloud changes.

This paper emphasizes the role of internal sea ice processes in determining the sea ice–albedo feedback mechanism over the Arctic pack ice. We focus on the processes that determine surface albedo and associated

Corresponding author address: Dr. Judith A. Curry, Department of Aerospace Engineering Sciences, Campus Box 429, University of Colorado–Boulder, Boulder, CO 80309-0429.

feedback mechanisms in multiyear pack ice in an attempt to assess the stability of the pack ice in the central Arctic Ocean. We use the one-dimensional sea ice models described by Curry and Ebert (1992), Ebert and Curry (1993), and Schramm et al. (1994) to assess the strength of the local sea ice–albedo feedback mechanism over the Arctic ice pack and the important physical processes that must be included to correctly incorporate the sea ice–albedo feedback mechanism into climate models. The results from this model are compared with those from the Semtner (1976) level-0 and level-3 models and the Maykut and Untersteiner (1971) model.

2. Model description

A one-dimensional sea ice model is employed, having a sophisticated surface albedo parameterization that is highly sensitive to the surface state and allows complex spectral radiative interactions to occur between the sea ice and the atmosphere. A "slab" version of this model has been described by Ebert and Curry (1993) and Curry and Ebert (1992) that includes the following features: specified ice divergence that allows for ice export; a lead parameterization that includes lateral ablation and accretion; ocean heat flux that is tied to warming of the ocean mixed layer by the penetration of solar radiation through the ice and in leads; a melt pond parameterization that allows for pond runoff and a variable pond area and depth; and an interactive surface albedo parameterization. Five surface types are included in the model: new snow, melting snow, bare ice, meltwater ponds, and open water. The albedo parameterization includes spectral discretization into four spectral intervals and dependence on the solar zenith angle, ratio of direct to diffuse radiation, and cloud properties. The seasonal cycle of baseline surface fluxes are specified in this study using the results described by Curry and Ebert (1992) and Ebert and Curry (1993).

The Ebert and Curry (1993) model has been modified to include an ice thickness distribution following Bjork (1992). The basic idea behind the ice thickness distribution model is that the sea ice is resolved into a limited number of ice classes that are characterized by their thicknesses and areas. Thin ice categories participate in the ridging process, transferring some ice to the thickest category; otherwise each class of ice evolves thermodynamically, independently from the others. New ice classes are continuously created by freezing of water in leads, with classes of similar thicknesses then merged to prevent the number of ice classes from becoming excessive. In this paper, a maximum of $n = 10$ ice thickness categories are used; $n = 1$ corresponds to the slab model described by Ebert and Curry (1993). The sea ice is further divided into first year (FY) and multiyear (MY) ice. The sea ice thermodynamics included in the slab model were modified in the following way for the ice thickness distribution model, using data described by Grenfell and Maykut (1977) and Grenfell (1983): (i) inclusion of spectral extinction coefficients in ice and snow that decrease with melting, ice age (FY or MY), and the amount of brine trapped in the sea ice; (ii) enhanced spectral absorption in a 5-cm granular layer atop bare ice, producing surface melting; (iii) transmission of solar radiation through snow; (iv) specification of melt pond areal coverage as a function of ice age and pond age, with FY ice having significantly greater pond coverage; and (v) melt pond albedo calculated as a function of both pond thickness and ice thickness. The annual cycles of modeled surface albedo, temperature, and radiation fluxes, along with ice characteristics including ice thickness, lead fraction, and pond characteristics, show good agreement with available observations (Curry and Ebert 1992; Ebert and Curry 1993).

The annual cycle of modeled surface albedo for the baseline surface fluxes are shown in Fig. 1 for both $n = 1$ and $n = 10$, corresponding to a latitude of 80°N. The minimum albedo for the $n = 10$ simulation is slightly higher than that for the $n = 1$ simulation because pond depth is limited for the thinner ice categories. The albedo difference in autumn arises from more rapid freezing of leads and the creation of thin ice. The autumnal surface albedo for the $n = 10$ simulation agrees better with the limited observations of autumnal surface albedo (as summarized by Ebert and Curry 1993). The significant events in the Arctic that contribute to variations in the surface albedo are shown in Fig. 1. By the end of May most of the snowfall has ceased, and the albedo decreases to the aging snow value. Several days later the snow begins to melt and the albedo decreases to the melting snow value. In mid July all the snow has melted except over the thickest ice categories, leaving bare ice. The albedo reaches its minimum when the melt pond fraction is at a maximum. In August, the melt ponds have refrozen and the albedo increases to the bare ice value, and the surface temperature begins its autumn cooling. The leads

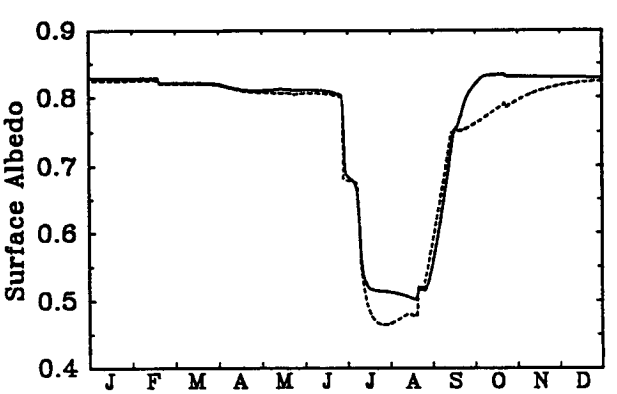

FIG. 1. Annual cycle of surface albedo for $n = 1$ (dash) and $n = 10$ (solid).

begin to freeze over and the snow begins to accumulate in September, the albedo returning to the new snow value.

Figure 2 shows the relationship between surface albedo and surface temperature over the annual cycle. During winter when the sun is absent, surface albedo is undefined. During the summer melt season, surface temperature remains constant while surface albedo decreases. During the low sun months, surface albedo remains relatively constant while surface temperature varies with insolation. During the transition seasons, surface albedo decreases as surface temperature decreases. Clearly, the surface albedo of the sea ice is not constant over the annual cycle (e.g., as assumed by Thorndike 1992) nor is the surface albedo a linear function of surface temperature (e.g., as assumed by Ledley 1991; Harvey 1988).

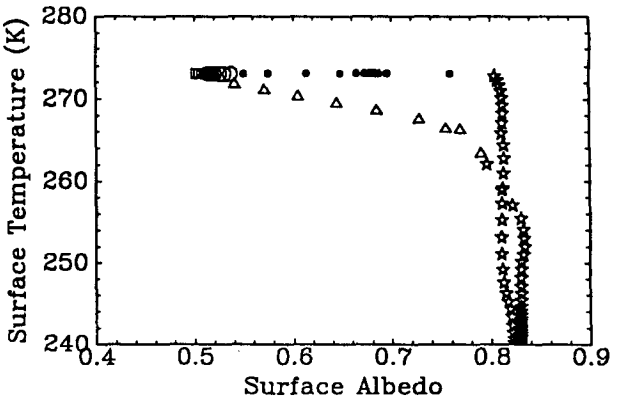

FIG. 2. Scatterplot of the annual cycle of surface albedo vs surface temperature. The symbols are as follows: stars are wintertime snow cover, plotted every 4 days; closed circles are melting snow, plotted every day; open circles are melting ice, plotted every day; squares are ponds freezing, plotted every 4 days; and triangles are accumulating snow, plotted every 3 days.

3. Sensitivity to surface flux perturbations

The climate forcing for these experiments is chosen to be a perturbation to the surface infrared radiation heat flux, simulating the effect of an increase in atmospheric CO_2. This method of forcing a one-dimensional model has been used to study atmospheric feedback processes by Schneider (1972), Cess (1975), Paltridge (1980), among others. In the perturbed experiments, atmospheric temperature, humidity, and cloud properties remain the same as in the baseline experiment; cloud and water vapor feedbacks are inoperative and the effects of the sea ice–albedo feedback mechanism can be isolated. The temperature–radiation feedback (negative), associated with a change in upwelling infrared flux due to a change in surface temperature, has been included. To obtain the annually averaged surface temperature and ice thickness for a given surface forcing, the model is run for 100 years, and the results are averaged for the last 50 years of integration. In the $n = 1$ simulations, it is noted that equilibrium, as defined by less than 1 mm change in ice thickness, was frequently attained before 100 years of integration; in this case the equilibrium values are used.

The annual cycle of surface temperature, albedo, and sea ice thickness are compared in Fig. 3 for the baseline and perturbed calculations ($\Delta F = \pm 5$ W m^{-2}) for both the $n = 1$ and the $n = 10$ versions of the model. This value of the surface forcing may be compared to the direct $2 \times CO_2$ forcing of 4 W m^{-2} (e.g., Ramanathan et al. 1989). For ± 5 W m^{-2} perturbation in the $n = 1$ simulation, the annually averaged surface warming is 4.0°C and the surface cooling is 2.3°C; By contrast, the $n = 10$ simulation shows an annually averaged surface temperature change of ±1.5°C. The asymmetry with respect to the sign of the surface flux perturbation in the $n = 1$ model arises from the fact that as the ice thins below 2 m in depth, the modeled surface albedo increases with decreasing ice depth toward open water values (Ebert and Curry 1993), accelerating the albedo feedback. The reduced sensitivity of the $n = 10$ model to a surface flux perturbation arises from the impact of the ice thickness distribution on the sea ice thermodynamics, as the relatively rapid growth of the thin ice categories and subsequent ridging acts to stabilize the ice thickness.

Table 1 compares values of the surface heat flux perturbation required to completely melt the ice during summer (warm transition) and the perturbation required to maintain yearround snow cover (cold transition) for the $n = 1$ and $n = 10$ simulations. Also included are equivalent results for the Maykut and Untersteiner (1971) model, the Semtner (1976) level-0 and level-3 models, and the Thorndike (1992) toy model. In conducting these experiments, the same baseline (zero perturbation) surface fluxes were used for all the models, and the ocean flux was tuned slightly to yield the same equilibrium sea ice thickness under the baseline forcing. Surface flux perturbations required to reach the cold transition range from -16 W m^{-2} for the Semtner level-0 model to -23 W m^{-2} for the Semtner level-3 model. Values of surface flux perturbation required to reach the warm transition show considerable variability, ranging from 3 to 20 W m^{-2}; the $n = 1$ Maykut and Untersteiner (1971) and the Semtner level-3 models reach this transition for the lowest surface flux perturbations. Differences between these models arise not only from different treatments of the ice–albedo feedback, but from other model processes as well. The differences between the transitions for the $n = 1$ and $n = 10$ versions of the model arise solely from the effects of including the ice thickness distribution. The differences between the Semtner level-0 and level-3 models arise primarily from the impact of model resolution on the treatment of conduction. It is interesting to note that the $n = 10$ results, which include the most complete

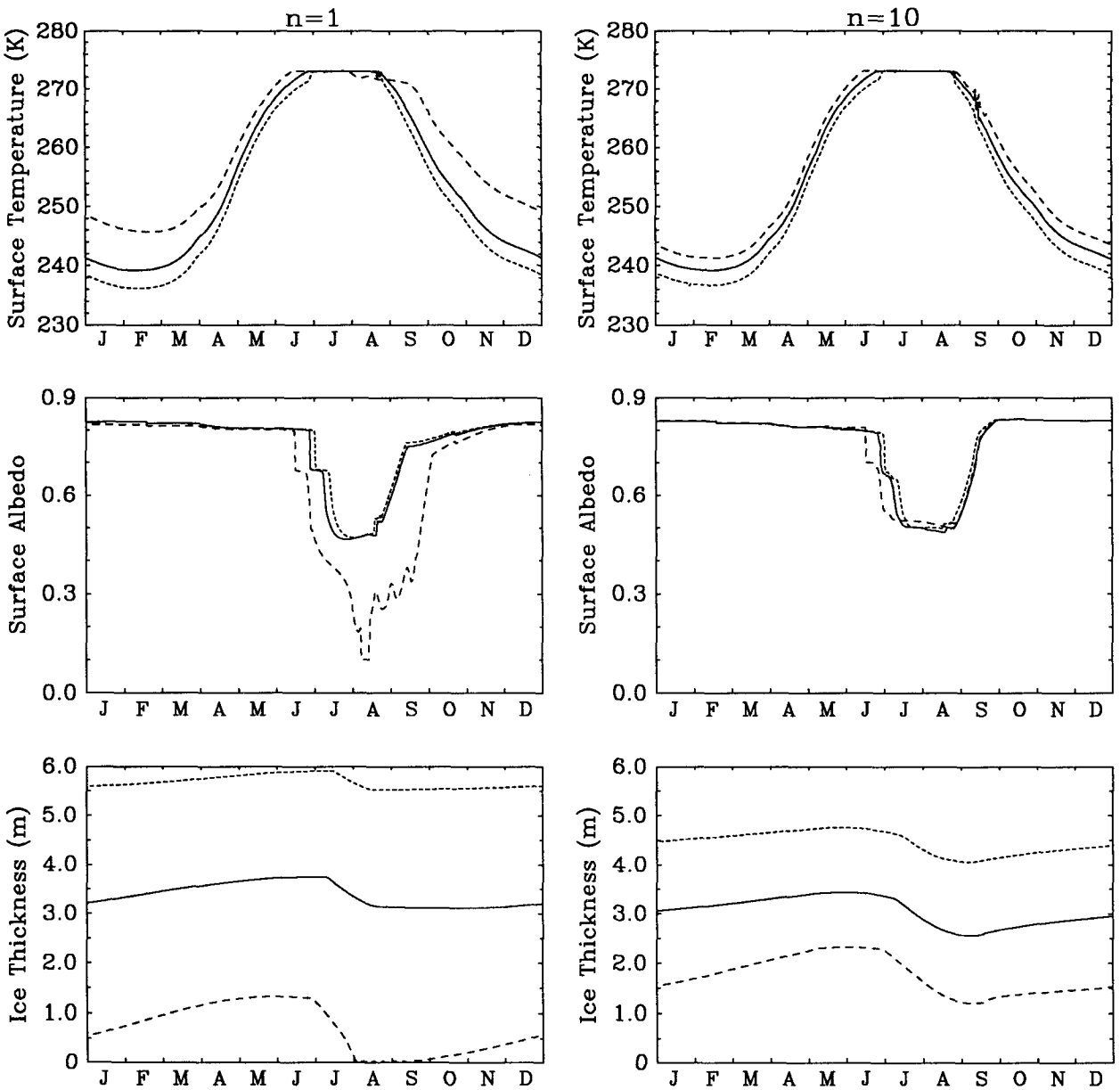

FIG. 3. Annual cycle of (a) surface temperature, (b) surface albedo, and (c) sea ice thickness. The following heat flux perturbations (ΔF) are examined for simulations that include the ice-albedo feedback: (solid) $\Delta F = 0$, (dash) $\Delta F = +5$ W m^{-2}, (dot) $\Delta F = -5$ W m^{-2}.

treatment of sea ice physics, are most nearly approximated by the Semtner level-0 model.

4. Sea ice–albedo feedback

To assess the strength of the sea ice–albedo feedback for the different models, we compare perturbed simulations that include the ice–albedo feedback with the corresponding perturbed simulation that does not include ice–albedo feedback. For the simulations that do not include the ice–albedo feedback, the annual cycle of the surface albedo remains fixed at the baseline simulation for the individual model (as shown in Fig. 1). Figure 4 shows the annually averaged values of surface temperature (Fig. 4a), surface albedo (Fig. 4b), and ice thickness (Fig. 4c) as a function of the surface heat flux perturbation for both the $n = 1$ and $n = 10$ versions of the model. As expected for a surface heat flux increase, surface temperature increases, surface albedo decreases, and sea ice thickness decreases. Comparison of the $n = 1$ (thin) with $n = 10$ (bold) simulations shows that the slopes of the $n = 1$ lines are steeper, reflecting the greater sensitivity of the $n = 1$ model to surface forcing.

TABLE 1. Infared heat flux perturbation at which the transition to yearround snow cover and summertime disappearance of sea ice occurs for models described in text.

Case	Yearround snow (W m^{-2})	Ice melts in summer (W m^{-2})
EC		
n = 1	−17	3
n = 10	−17	8
MU	−17	4
Semtner		
level-0	−16	11
level-3	−23	5
Thorndike	−20	20

By comparing the solid lines (including ice–albedo feedback) with the dashed lines (excluding ice–albedo feedback) in Fig. 4, it is seen that the perturbations for surface temperature and ice thickness are generally greater for the cases that include the ice–albedo feedback, indicating a positive feedback. The relative slopes of the solid lines (include ice–albedo feedback) and the dashed lines (no ice–albedo feedback) are larger for the $n = 1$ model, indicating that the strength of the sea ice–albedo feedback mechanism is greater for the $n = 1$ model than for the $n = 10$ model. Significant changes in the slope of the lines are seen at the warm and cold transitions.

The strength of the sea ice–albedo feedback may be quantified by defining the feedback parameter S:

$$S(X) = \Delta X_\alpha / \Delta X - 1, \qquad (1)$$

where X is the climate parameter (annually averaged surface temperature, T_s, or ice thickness, h_i), Δ denotes the change in X associated with a specified forcing, and the subscript α indicates that ice–albedo feedback mechanism is included. A positive value of $S(X)$ indicates a positive ice–albedo feedback mechanism; $S(X)$ varies with the sign and the magnitude of the forcing, although this variation is fairly small as long as the perturbed ice state is not near either the warm or cold transitions.

The calculated feedback parameters, $S(T_s)$ and $S(h_i)$, are shown in Fig. 5 for the different models shown in Table 1, where the open circles indicate the warming experiments and the closed circles indicate the cooling experiments. Here $S(X)$ is determined for a surface perturbation of ±2 W m^{-2} for all models except for the $n = 10$ model, where ±5 W m^{-2} is used. The large values of $S(X)$ for the warming perturbation for the $n = 1$ model reflects the fact that +2 W m^{-2} is close to the warm transition for this model (see Table 1). The large ice–albedo feedback for the $n = 1$ model arises primarily from the presence of melt ponds, as shown by the $n = 1$ simulation without ponds in Fig. 5. In the absence of melt ponds, the summertime surface albedo is constrained not to fall below 0.56, which decreases the albedo feedback. Inclusion of the ice thickness distribution markedly decreases the ice–albedo feedback, with $S(h_i) = 0.45$ for $n = 10$. In general, $S(T_s) \neq S(h_i)$, with values of $S(h_i)$ typically greater than $S(T_s)$. Greater asymmetry between warming and cooling perturbations is seen for $S(h_i)$. Variations in $S(X)$ between the Semtner level-0 and level-3 models

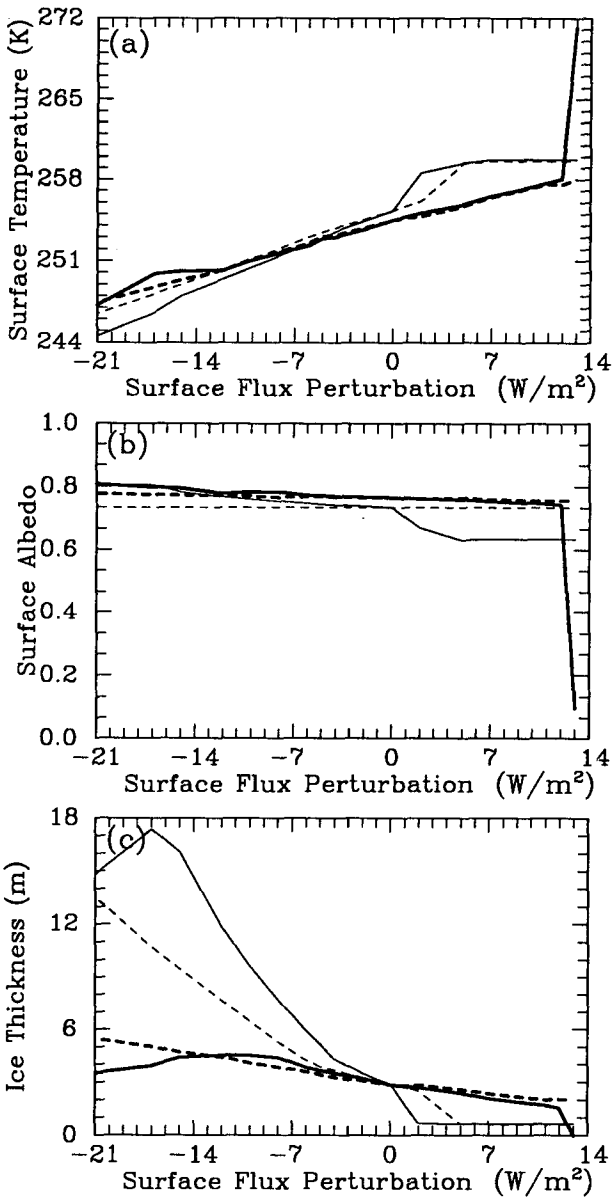

FIG. 4. Annually averaged values of (a) surface temperature, (b) surface albedo, and (c) ice thickness as a function of surface flux perturbation (ΔF). Solid curves represent the inclusion of the ice–albedo feedback, and dashed curves indicate the absence of ice–albedo feedback. Results are presented for the thickness distribution model with $n = 10$ (bold) and the slab model of Ebert and Curry (1993) ($n = 1$; thin).

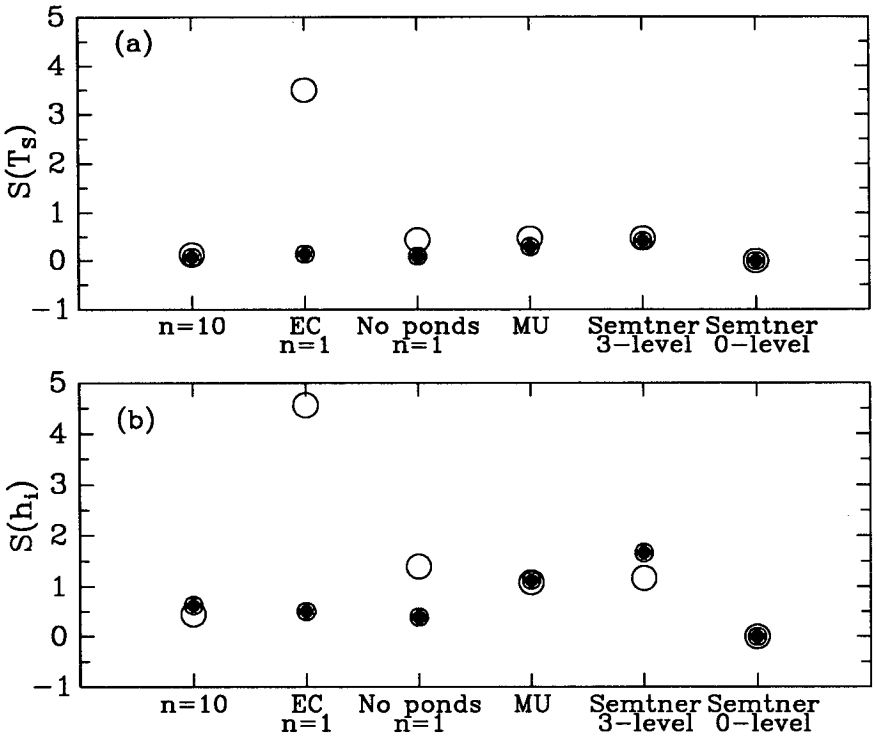

FIG. 5. The ice–albedo feedback, $S(X)$, as determined for (a) surface temperature and (b) ice thickness, for the experiments described in Table 1 (warming perturbation, open circles; cooling perturbation, closed circles).

arise from the impact of different vertical resolution on the conduction process, which puts each model in a different position relative to the warm and cold transitions for a ± 2 W m^{-2} perturbation. Variations in $S(X)$ between the $n = 1$ and $n = 10$ models are a result of the impact of the ice thickness distribution that make the $n = 10$ model less sensitive to a surface flux perturbation.

5. Discussion and conclusions

In its simplest form, the ice–albedo feedback mechanism is thought to be associated with a decrease in the areal cover of snow and ice and a corresponding increase in the surface temperature, further decreasing the areal cover of snow and ice. This vision of the ice–albedo feedback mechanism has been described by the ice–albedo feedback diagram shown by Kellog (1973), which included only the ice–albedo feedback associated with ice extent. We have shown in this paper that the sea ice–albedo feedback can operate even in multiyear pack ice, without the disappearance of this ice, associated with internal processes occurring within the multiyear ice pack. This vision of the sea ice–albedo feedback mechanism is represented schematically in Fig. 6. In this figure the sea ice–albedo feedback mechanism is separated into two aspects: 1) the sea ice edge albedo feedback, associated with changes in horizontal extent of the sea ice; and 2) the sea ice pack albedo feedback mechanism, associated with internal processes occurring within the multiyear ice pack (e.g., duration of the snow cover, ice thickness, lead fraction, ice thickness, and melt pond characteristics). The sea ice pack albedo mechanism is described as follows. A perturbation to the surface energy balance of the sea ice results in a perturbation to surface temperature, melt pond and lead fraction, snow depth, ice thickness, and other sea ice characteristics. Changes in melt pond and lead fraction, snow depth, and sea ice thickness alter the surface albedo, which changes the surface energy balance. It is important to point out that this interpretation of the sea ice–albedo feedback depends on the spatial and temporal scales of the changes under consideration. Because of time lags in the sea ice system, it is essential to consider how the sea ice–albedo feedback mechanism operates when integrated through at least a full seasonal complete annual cycle.

In our determination of the ice–albedo feedback mechanism, we compared calculations that included the ice–albedo feedback mechanism with calculations that did not include this feedback mechanism. To specifically examine the ice–albedo feedback mechanism, we chose a surface infrared heat flux perturbation for the forcing and excluded any atmospheric feedback processes (e.g., water vapor feedback, cloud feedback).

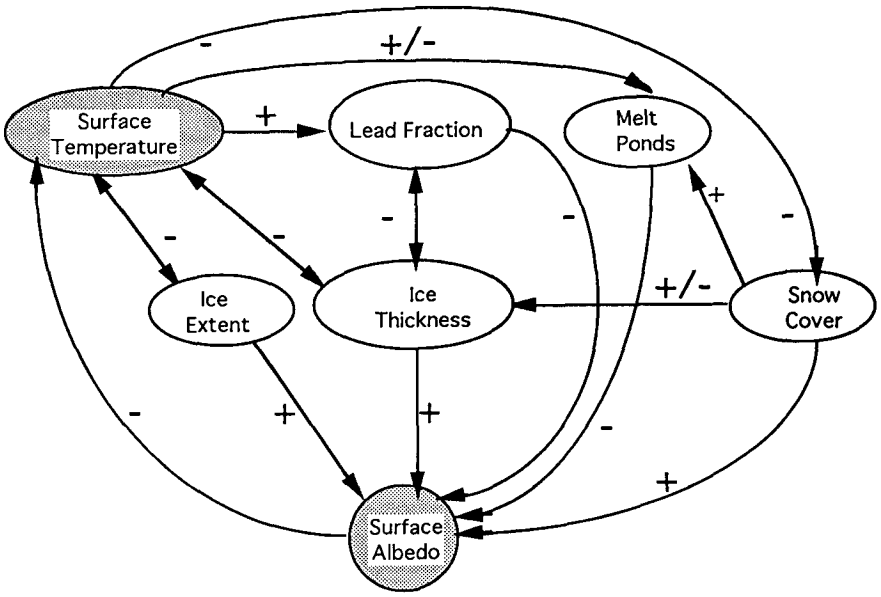

FIG. 6. Schematic diagram of the sea ice–albedo feedback mechanism. The direction of the arrow indicates the direction of the interaction. A "+" indicates a positive interaction (an increase in the first quantity leads to an increase in the second quantity) and a "−" indicates a negative interaction (an increase in the first quantity leads to a decrease in the second quantity). A "±" indicates either that the sign of the interaction is uncertain or that the sign changes over the annual cycle.

For a given model, the ice–albedo feedback was shown to vary with the strength of the perturbation, particularly as the warm or cold transition was approached; the feedback parameter defined in terms of ice thickness was typically greater than that defined in terms of surface temperature. In a comparison of a number of different one-dimensional sea ice models that have the same annually averaged sea ice thickness for present-day surface forcing, it was shown that there is a substantial difference between the models in terms of sensitivity to surface heat flux perturbations and ice-albedo feedback. The Semtner level-3, Maykut and Untersteiner, and Curry and Ebert "slab" models were shown to be very sensitive to warming perturbations, showing complete summertime melting of the sea ice for surface flux perturbations ranging from 3 to 5 W m^{-2}. The ice thickness distribution model and Semtner level-0 model showed reduced sensitivity to warming perturbations; the ice thickness distribution model showing complete summertime ice melt only for surface heat flux perturbations ≥ 8 W m^{-2}. It is ironic that the sensitivity of the ice thickness distribution model, which contains the most complete treatment of sea ice physics, is most nearly approximated by the Semtner level-0 model, which contains the crudest treatment.

Which model has the most correct treatment of ice-albedo feedback? It is difficult to say. The ice thickness distribution model contains the most complete sea ice physics. However, the Ebert and Curry slab model has the next most complete sea ice physics and shows vastly different sensitivities than does the ice thickness distribution model. Simply because the ice becomes thinner (or the surface warmer) for a given surface flux perturbation does not imply a stronger ice–albedo feedback mechanism; other processes than ice–albedo feedback may contribute to this sensitivity. The ice–albedo feedback mechanism appears to be particularly sensitive to melt ponds, the ice thickness distribution, and the treatment of conduction within the ice (i.e., vertical resolution, temperature and salinity dependence of the thermal diffusivity). Additional improvements to our understanding of the ice–albedo feedback mechanism require improved treatment of ice thickness distribution, ice dynamics, and ocean–sea ice coupling, in addition to processes that directly impact surface albedo, such as melt ponds. An improved database for sea ice thermodynamics is required to validate the model and to provide the basis for improved model parameterizations. In assessing the performance of a sea ice model, it is important to consider the sensitivity of the model to surface heat flux perturbations.

In this paper we have focused only upon one feedback mechanism that affects the stability of the Arctic Ocean sea ice, namely the ice–albedo feedback. The overall stability of the Arctic Ocean pack ice depends upon the interrelationships among all of the feedback processes occurring in the coupled atmosphere–sea ice–ocean system.

Acknowledgments. This research has been supported by DOE NIGEC South Central Region and ONR

N00014-91-J-1387. Comments on the manuscript from N. Untersteiner and S. Warren are appreciated.

REFERENCES

Bjork, G., 1992: On the response of the equilibrium thickness distribution of sea ice to ice export, mechanical deformation, and thermal forcing with application to the Arctic Ocean. *J. Geophys. Res.*, **97,** 11 287–11 298.

Cess, R. D., 1975: Global climate change: An investigation of atmospheric feedback mechanisms. *Tellus,* **27,** 193–198.

Chapman, W. L., and J. E. Walsh, 1993: Recent variations of sea ice and air temperature in high latitudes. *Bull. Amer. Meteor. Soc.,* **74,** 33–47.

Curry, J. A., and E. E. Ebert, 1992: Annual cycle of radiation fluxes over the Arctic Ocean: Sensitivity to cloud optical properties. *J. Climate,* **5,** 1267–1280.

Dickinson, R. E., G. A. Meehl, and W. M. Washington, 1987: Ice-albedo feedback in a CO_2-doubling simulation. *Clim. Change,* **10,** 241–248.

Ebert, E. E., and J. A. Curry, 1993: An intermediate one-dimensional thermodynamic sea ice model for investigating ice-atmosphere interactions. *J. Geophys. Res.,* **98,** 10 085–10 109.

Grenfell, T. C., 1983: A theoretical model of the optical properties of sea ice in the visible and near infrared. *J. Geophys. Res.,* **88,** 9723–9735.

——, and G. A. Maykut, 1977: The optical properties of ice and snow in the Arctic Basin. *J. Glaciol.,* **18,** 445–463.

Harvey, L. D. D., 1988: Development of a sea ice model for use in zonally averaged energy balance climate models. *J. Climate,* **1,** 1221–1238.

Houghton, J. T., G. J. Jenkins, and J. J. Ephraums, 1990: *Climate Change: The IPCC Scientific Assessment.* Cambridge University Press, 365 pp.

Ingram, W. J., C. A. Wilson, and J. F. B. Mitchell, 1989: Modeling climate change: An assessment of sea ice and surface albedo feedbacks. *J. Geophys. Res.,* **94,** 8609–8622.

Kellog, W. W., 1973: Climatic feedback mechanisms involving the polar regions. *Climate of the Arctic,* G. Weller and S. A. Bowling, Eds., Geophysical Institute, Fairbanks, AK, 111–116.

Ledley, T. S., 1991: Snow on sea ice: Competing effects in shaping climate. *J. Geophys. Res.,* **96,** 17 195–17 208.

Maykut, G. A., and N. Untersteiner, 1971: Some results from a time dependent thermodynamic model of sea ice. *J. Geophys. Res.,* **76,** 1550–1575.

Paltridge, G., 1980: Cloud radiation feedback to climate. *Quart. J. Roy. Meteor. Soc.,* **106,** 895–899.

Ramanathan, V., R. D. Cess, E. F. Harrison, P. Minnis, B. R. Barkstrom, E. Ahmad, and D. Hartman, 1989: Cloud-radiative forcing and climate: Results from the Earth Radiation Budget Experiment. *Science,* **243,** 57–63.

Schneider, S. H., 1972: Cloudiness as a global climatic feedback mechanism: The effects on the radiation balance and surface temperature of variations in cloudiness. *J. Atmos. Sci.,* **20,** 1413–1422.

Schramm, J. L., E. E. Ebert, and J. A. Curry, 1994: Disposition of solar radiation in sea ice and the upper ocean. Preprints, *Eighth Conf. on Atmospheric Radiation,* Nashville, TN, Amer. Meteor. Soc., 73–75.

Semtner, A. J., Jr., 1976: A model for the thermodynamic growth of sea ice in numerical investigations of climate. *J. Phys. Oceanogr.,* **6,** 379–389.

Spelman, M. J., and S. Manabe, 1984: Influence of oceanic heat transport upon the sensitivity of a model climate. *J. Geophys. Res.,* **89,** 571–586.

Thorndike, A. S., 1992: A toy model of sea ice growth. *Modeling the Earth System,* D. Ojima, Ed., 225–238. [Available from UCAR Office for Interdisciplinary Earth Studies Global Change, Boulder, CO.]

Washington, W. W., and G. A. Meehl, 1986: General circulation model CO2 sensitivity experiments: Snow-sea ice albedo parameterizations and globally averaged surface air temperature. *Clim. Change,* **8,** 231–241.